TOMBALL TECHNOLOGY CENTER

PETROLOGIC ANALYSIS OF WHOLECORE SEGMENTS

EQUITABLE PRODUCTION COMPANY
KANAWHA #1641
KANAWHA AND FAYETTE COUNTY, WV
WIER FORMATION

TECHNOLOGY CENTER REPORT NO. 04-02-0104

BJ SERVICES TECHNICAL REPRESENTATIVE

MR. ROGER MYERS

PITTSBURG, PA

JUNE 22, 2004

OBJECTIVES:

Conventional wholecore samples from the subject well were submitted to the Geological Services Group at the Tomball Technology Center for rock/pore properties characterization. The objectives of this analysis were to characterize framework mineralogy, cements, clays, and porosity types present in the sample, and identify potential completion problems. Analyses conducted were stereomicroscopy, acid solubility, scanning electron microscopy/energy dispersive spectrometry (SEM/EDS), and X-ray diffraction (XRD).

Samples from this project were also tested in the Rock Mechanics Laboratory for values of Young's Modulus and Poisson's Ratio. That work is in progress and will be reported separately.

SAMPLE ANALYSIS:

Two boxes of wholecore samples were shipped to Technical Services in Tomball for evaluation. Prior to analytical testing, the wholecore segments were photographed for documentation. The photographs are seen in Appendix I. Note that portions of the wholecore segments contained many small, horizontal shale laminations between "clean" sandstone layers (particularly 1965-66'). These thin shale laminations would probably be below the detectable limits of wireline logging tools.

Coreplugs were drilled from the wholecore segments where possible. Ten coreplugs from the upper segment (1965-1967.5') and three coreplugs from the lower interval (2020-2022.5') were obtained for porosity/permeability analysis. Results are included in the table below for reference. A permeability versus porosity crossplot (see Figure #1) was generated to better evaluate the data.

Table #1 - Routine Core Analysis Data

Weir Formation	Depth Ft	Gas Perm md.	Porosity %	Grain Density gm/cc
Upper Sand	1966.0'	0.37	10.4	2.642
	1966.1'	1.74	12.4	2.636
	1966.2'	1.13	12.2	2.638
	1966.8'	2.71 *(*fractured)*	8.6	2.750 *
	1966.9'	0.23	10.2	2.633
	1697.0'	0.12	9.4	2.638
	1967.1'	0.76	9.4	2.646
	1967.3'	0.08	8.2	2.649
	1967.4'	<0.01	2.3	2.680
	1967.5'	<0.01	1.6	2.690
Lower Sand	2021.0'	0.12	7.2	2.629
	2021.2'	0.73	8.1	2.624
	2022.0'	1.98	14.0	2.620

**** - the sample from 1966.8' contained a large clast that was microfractured.***

Figure #1 - Permeability versus Porosity Crossplot

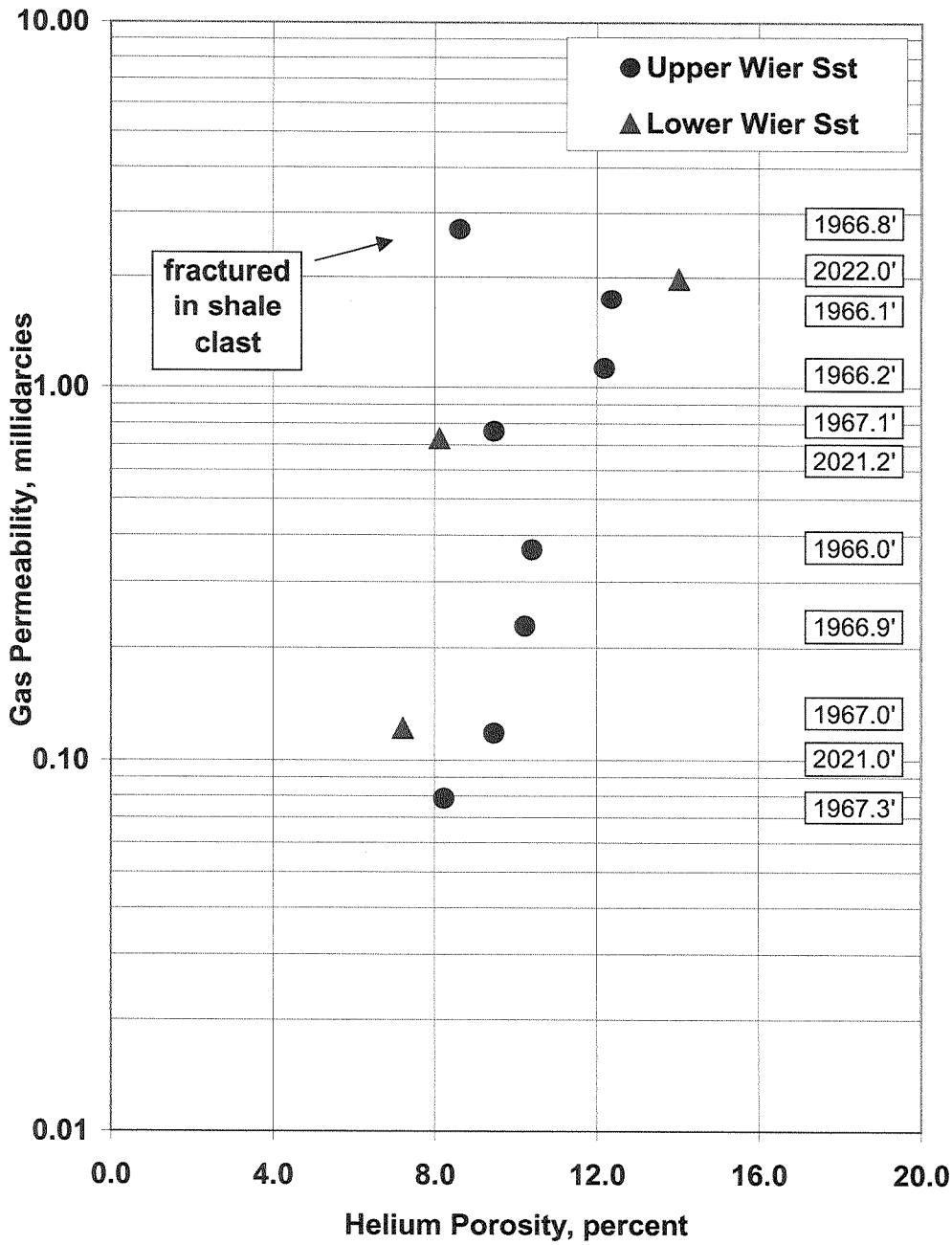

The data from the coreplug drilled at 1966.8' differed significantly from the other coreplugs drilled from the same wholecore segment, i.e., the grain density was much higher, the porosity was lower, and the gas permeability was much higher. Microfractures within a large brown clast within the 1966.8' coreplug are believed to account for the higher permeability. The lower porosity appears to be due to the significantly lower porosity seen in the clast, and the grain density (2.75 gm/cc) also is believed to be caused by the clast. A sub-sample of the clast was

prepared for XRD analysis, to determine the mineralogy of the clast. This analysis indicates that the clast is primarily siderite (iron carbonate), with secondary amounts of fluorapatite (calcium phosphate), quartz, and clays. Traces of pyrite (iron sulfide) were also noted in the XRD diffractogram of the clast. The abundance of iron-bearing minerals (siderite and pyrite) in the coreplug is the cause of the shift in grain density from approximately 2.65 to 2.75 gm/cc.

Lithological Descriptions

Table #2 - Lithological Descriptions

Weir Sand	Depth Ft	Descriptions
Upper Sand	1966.0'	Sandstone, tan, very fine- to fine-grained, well-sorted, well-indurated.
	1966.1'	(as above)
	1966.2'	(as above)
	1966.8'	(as above, with large brown clast)
	1966.9'	Sandstone, tan, very fine- to fine-grained, well-sorted, well-indurated.
	1697.0'	(as above)
	1967.1'	(as above)
	1967.3'	(as above)
	1967.4'	Sandstone, light-gray, very fine- to fine-grained, well-sorted, very well-indurated, very calcareous.
	1967.5'	(as above)
Lower Sand	2021.0'	Sandstone, tan, very fine- to fine-grained, well-sorted, well-indurated, small shale clasts.
	2021.2'	(as above, with small clay drapes)
	2022.0'	Sandstone, tan-brown, very fine- to fine-grained, well-sorted, well-indurated, faintly-laminated.

Mineralogical Analysis

Four samples were selected to represent the two intervals: Sub-samples were selected for mineralogical definition (XRD analysis) and rock/pore network characterization (SEM analysis). Sub-samples were also taken for acid solubility and soluble iron content.

Acid solubility was conducted using 15% hydrochloric acid on disaggregated material for one hour at 90°F. X-ray techniques are used to determine the crystalline material content of samples. Interpreted minerals and their relative percentages are shown in Figure #2 and Table #3.

Figure #2 - Mineralogical Data Ribbon Chart

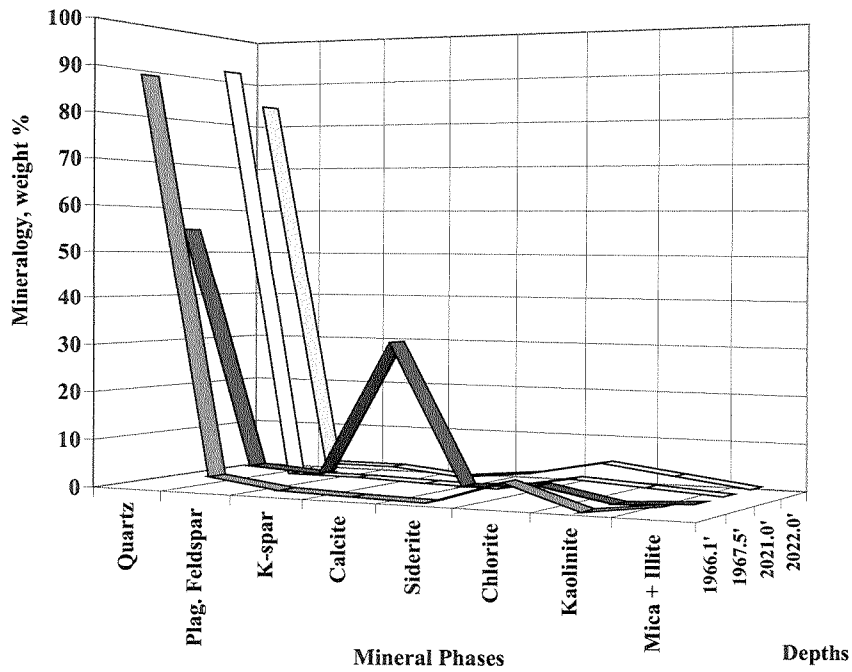

Table #3 - Mineralogical Analysis (XRD results in weight percents) & Solubility Testing

Formation Components	Mineral Phases	1966.1'	1967.5'	2021.0'	2022.0'
Framework Grains & Quartz Cement	Quartz (SiO_2)	88	55	91	84
	Plagioclase Feldspar	3	4	1	2
	Potassium Feldspar	1	3	1	2
Carbonates	Calcite ($CaCO_3$)	*trace*	31	*trace*	*trace*
	Siderite ($FeCO_3$)	---	2	---	2
Clays	Kaolinite	---	---	2	3
	Chlorite	5	3	3	5
	Mica + Illite	2	1	1	1
TOTALS		100%	100%	100%	100%
ACID SOLUBILITY TESTING					
15% HCl Solubility (%)		4	10	3	1

Scanning Electron Microscopy

Formation chips were cleaned with hydrocarbon solvents and dried in a convection oven. Fresh surfaces were obtained by cracking the chips open; these pieces were subsequently mounted on aluminum sample holders for SEM/EDS analysis. The attached SEM photoplates document the rock/pore network seen in these samples, and illustrate specific examples of common features at varying magnifications.

1966.1', 2021-2022'

These fine- to very fine-grained, well-sorted sandstones are clay-cemented and composed primarily of quartz, plagioclase and potassium feldspar framework grains. Quartz overgrowths, grain-coating clays, and traces of authigenic calcite contribute to cementation and porosity reduction. Intergranular porosity is described as Fair, due to the presence of a network of small intergranular pores that have not been entirely filled by the grain-coating clays and calcite cement. Microporosity is extensive. Authigenic chlorite is the primary clay with illite and kaolinite (noted in the 2021-2022' samples) also present. Secondary porosity created by the partial-dissolution of the feldspars slightly effects an increased total porosity, but a significant portion of this secondary porosity is classified as microporosity (See Photoplate I, View B). This is due to the dissolution porosity being associated with the leaching of feldspar cleavage planes, rather than dissolution of the entire grain leaving grain-sized pores.

1967.5'

This calcareous, fine- to very fine-grained sandstone contains quartz, plagioclase feldspar, and potassium feldspar framework grains. Intergranular porosity for this sample is described as Poor due to the abundance of carbonate cement. Calcite is both the primary cementing material and the primary porosity-reducer. Authigenic siderite is also present in minor amounts. The presence of grain-coating chlorite and illitic clays are minimal and contribute to porosity reduction.

The framework grains in both of these Weir Sandstone zones are coated with variably-thick layers of authigenic chlorite. The chlorite occurs in the classic bladed form, creating abundant microporosity between the chlorite platelets, with associated high irreducible water saturations in the reservoir. In addition to the porosity reduction and microporosity associated with the bladed chlorite, the iron content in the chlorite can have a significant impact on wireline log data. As a conductive mineral, chlorite impacts resistivity measurements, shifting resistivities lower and affecting calculated water saturations. Also, if the higher grain density of chlorite-rich sandstones is not accounted for in density porosity calculations, the wireline log porosity values may be erroneously high.

POTENTIAL COMPLETION PROBLEMS:

Listed in the table below are the potential completion problems noted in these samples. Discussion of these completion problems follows the table, **in order of importance**.

Table #4 - Potential Completion Problems

DEPTH	MATRIX RESERVOIR QUALITY	FLUID RETENTION?	FINES MIGRATION?	SWELLING CLAY SENSITIVITY?	HCl ACID SENSITIVE?
1966-67'	Fair	Yes	No	No	Moderately, due to the presence of grain-coating chlorite clay.
1967.5'	Poor	No			
2021-22'	Fair	Yes, due to presence of microporosity.	Slightly, due to the presence of kaolinite booklets.		

- Matrix Reservoir Quality
  The reservoir quality of the 1966-67' and 2021-22' intervals are characterized as Fair, due to the presence of small open intergranular pore spaces and thin coating of grain-coating chlorite and illitic clays. Due to heavy carbonate cementation in the sample from 1967.5', intergranular porosity is described as Poor.

- Natural Fractures
  Dessication fractures were noted in a siderite clast within one of the coreplugs, but were isolated within the clast and would therefore have no impact on reservoir permeability.

- Water Sensitivity - Fluid Retention in Microporosity
  Because capillary forces are strong in microporosity, injected fluids may tend to be retained in these pore spaces. This has the effect of increasing water saturation (assuming that these pores are not already saturated with interstitial formation water). Increasing water saturation decreases relative permeability to hydrocarbons, thus reducing hydrocarbon deliverability. See **Appendix I** for an extended discussion of this phenomenon, also known as aqueous phase trapping.

- Acid Sensitivity
  Treatment of chlorite-rich reservoirs (or other iron-rich minerals such as siderite) with HCl-based acid blends may lead to multiple types of permeability reduction.
  1) Removal of chlorite's iron may cause disintegration of the clay structure, leaving an amorphous silicate residue which may migrate and precipitate when the pH of the acid increases. This amorphous silicate can therefore lower reservoir permeability..
  2) HCl leaching of iron from the chlorite puts ferrous iron (Fe^{+2}) into solution. If the pH of the spent solution approaches pH of 7, colloidal ferric hydroxide ($Fe[OH]_3$) may form and precipitate in the rock/pore network. This gelatinous material can plug reservoir permeability and lower deliverability.

- Mud Acid Sensitivity
  Treatment of reservoirs containing abundant **calcareous minerals** and/or **feldspars** with *hydrochloric-hydrofluoric (HCl:HF)* blends may cause precipitation of secondary reaction products such as fluorite (CaF_2), and the hexafluorosilicates (K_2SiF_6), $CaSiF_6$, and Na_2SiF_6. These precipitates may cause severe reduction of permeability and therefore deliverability.

- Fines Migration
  Exposure of delicate authigenic clays to turbulent fluid flow during drilling, completion, or production may cause clay particles to become detached and to migrate through the pore network, bridging at narrow pore throats and reducing permeability. The presence of extremely fragile forms of pore-filling kaolinite booklets make this formation slightly susceptible to fines migration.

Technology Center Report No. 04-02-0104 Reported by: BJ Davis & Stephanie Jones

Requested by:	Roger Myers
Location:	Pittsburgh, PA
Analyzed by:	BJ Davis, Dr. Gerald Braun, Stephanie Jones, David Wang
Distribution:	Roger Myers, Daniel Kendrick, Marc Scholl, Randy LaFollette, Bill Wood, Formation File, TTC File

ANALYTICAL PROCEDURES:

Stereomicroscopy

Stereomicroscopy is a reflected light microscopy technique performed at relatively low magnifications, commonly 20X and 63X. This technique is used to assess rock textural parameters and to subsample large sample sets for other analyses such as scanning electron microscopy, thin section petrology, and X-ray diffraction.

Scanning Electron Microscopy/Energy Dispersive Spectrometry

Scanning electron microscopy/energy dispersive spectrometry (SEM/EDS) uses an electron beam generated in a vacuum chamber to image the sample. Samples are prepared by extracting volatile hydrocarbons and drying at low temperature. The cleaned and dried samples are subsequently sputter-coated with a 30 Angstrom thick layer of gold under vacuum. As the electron beam strikes the sample surface, topography sensitive secondary electrons are generated, collected in a detector, and computer imaged. X-rays are also generated while the sample is being scanned. The energy levels of these X-rays are characteristic of the elements from which they were generated. The X-ray energies are computer-imaged into an elemental (EDS) spectrum showing qualitative atomic composition of the sample. SEM/EDS techniques are used to provide both high and low magnification views of the sample with great depth of field, yielding interpretations of the interrelationships between grains, pore types, cements, and clays. SEM techniques are particularly useful in assessing the occurrence of clays within the pore network.

X-Ray Powder Diffraction

X-ray powder diffraction (XRD) is an analytical technique that bombards a finely-powdered rock sample with monochromatic Cuk_{α} radiation and measures intensity of the scattered beam versus 2-theta angle of the instrument. These data are used in the Bragg equation to calculate d-spacings of the material(s) present. *Bulk XRD samples* are prepared by mechanically grinding the sample to a fine powder and back-packing the powder into a hollow-cavity sample mount. *Clay samples* are prepared by separating the clay-size fraction from the bulk sample, and depositing a slurry containing the "clays" on a glass slide. Additional treatments of clay samples by glycolating (to distinguish smectite and expandable mixed-layer clays) and heat treating (to discern kaolinite from chlorite) are performed as needed. XRD is used to provide semi-quantitative data on the relative abundances of bulk and clay minerals present in rock samples analyzed. Such percentages are often critical to stimulation treatment design.

Acid Solubility Testing

Acid solubility testing involves digestion of a finely-sieved sample in excess 15% hydrochloric acid (HCl) at reservoir temperature for approximately 2 hours. Following digestion, the remaining sample is dried in a convection oven before obtaining a final sample weight and calculating weight loss (solubility) as a percent of initial sample weight. If appropriate, the acid-soluble iron content of the sample is also measured.

Routine Core Analysis

Helium porosities (ϕ) were determined by the Boyle's Law technique using a combination of the sample's grain volume and bulk volume. Cleaned and dried core plugs of known weight and

dimensions (bulk volume) were placed in a calibrated matrix cup. After expanding helium into the core plug to measure grain volume, the grain volume was subtracted from the bulk volume yielding porosity, reported as percent of bulk volume. Grain density was calculated as grain weight divided by grain volume and is reported in grams per cubic centimeter.

Gas permeability measured at ambient conditions is a specific permeability to gas (100% gas saturation). Cleaned and dried core plugs were inserted into rubber sleeves and placed in a core holder, where confining stress was applied to prevent gas bypass during permeability testing. Nitrogen gas was flowed through the plug until constant upstream and downstream pressures, and constant flow rate were obtained. Darcy's equation for laminar gas flow was used to calculate specific gas permeability.

Appendix I - Aqueous Phase Trapping Index

Hydrocarbon permeability reduction due to imbibition of aqueous treatment fluids has been well documented in the literature. This imbibition effect, also known as aqueous phase trapping, has been noted in both oil and gas reservoirs, and has been observed as a particularly severe problem in reservoirs where a sub-irreducible water saturation exists. Sub-irreducible water saturations are believed to have been created by a combination of factors, including dehydration, desiccation, compaction, mixed-wettability, significant height above the free water level in oil reservoirs, and diagenetic effects occurring through geologic time. Laboratory capillary pressure measurements supply good approximations of the irreducible water saturations that would normally be expected, but actual reservoir water saturations can be substantially lower, i.e., a sub-irreducible value. An example is the Alpine Field, west of Prudhoe Bay on the Alaskan Slope. Alpine reservoir water saturations are approximately 19%, but relative permeability data indicate that the expected irreducible water saturations should be 40-50%.[1]

Injection of aqueous fluids into sub-irreducible reservoirs results in the creation of a zone of high water saturation in the near-wellbore or near-fracture area. Subsequent hydrocarbon production results in the affected zone reverting to the irreducible water saturation dictated by the capillary mechanics of the system, rather than the sub-irreducible saturation created by dehydration, etc., over extended geologic time. The net effect is that the critical drawdown area of the well retains an increased water saturation, a lowered relative permeability to gas, and therefore poorer production characteristics.

Bennion et al. (1996)[2] developed an equation as a diagnostic tool to help evaluate a reservoir's sensitivity to aqueous phase trapping. The equation is based upon the zone's average permeability and initial water saturation values:

$$\mathbf{APT_i = 0.25[\log_{10}(K_a)] + 2.2(S_{wi})}$$

where $\mathbf{APT_i}$ is the Aqueous Phase Trap Index
$\mathbf{K_a}$ is the uncorrected average formation air permeability (millidarcies)
$\mathbf{S_{wi}}$ is the initial (not irreducible) water saturation (fraction)

APT_i values may range from zero to one, but more typically vary from 0.3-1.0. Table #I-1 below contains guidelines for interpretation of $\mathbf{APT_i}$ values.

Table #I-1 - APT Index Values and Corresponding Reservoir Characteristics

APT_i Range	Reservoir Characteristics
$APT_i \geq 1.00$	formation **unlikely** to exhibit significant permanent sensitivity to aqueous phase trapping
$0.80 \leq APT_i \leq 1.00$	formation **may exhibit** sensitivity to aqueous phase trapping
$APT_i < 0.80$	formation **will likely exhibit** significant sensitivity to aqueous phase trapping

Figure #I-1 is a crossplot modified from the Bennion, et.al. paper showing air permeability plotted versus the initial water saturation, illustrating the APT_i ranges.

Figure # I-1 - Illustration of APT_i Correlations (modified from Bennion, et.al.)

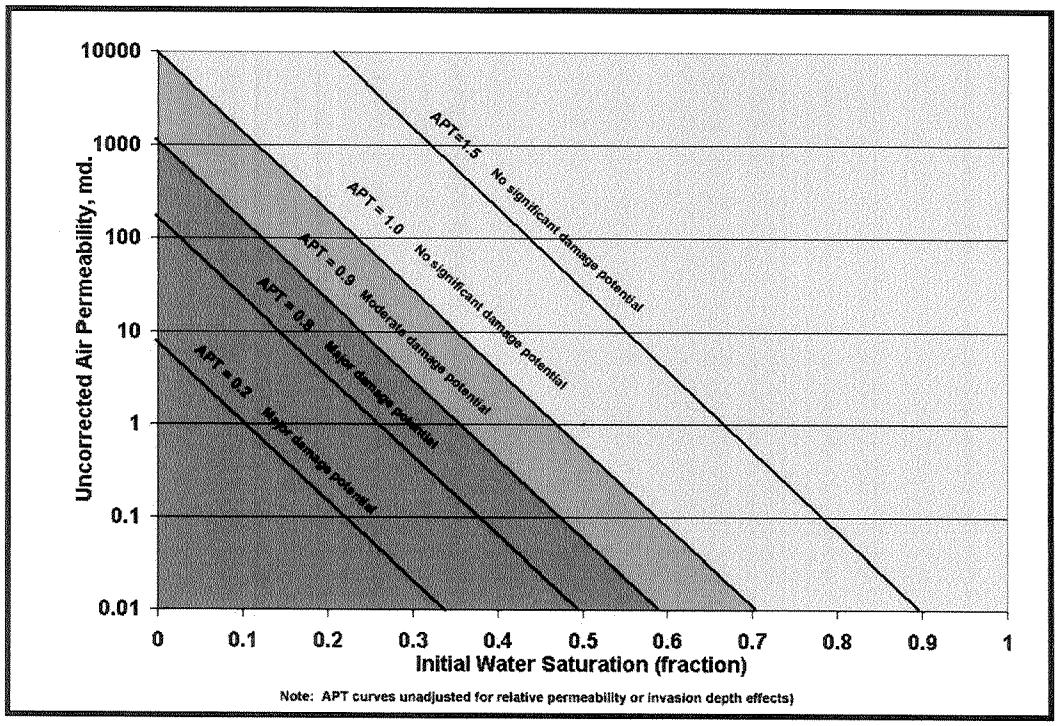

Table #I-2 presents values of APT_i calculated with water saturations decreasing from 70% to 10%, at four permeability levels (0.001, 0.01, 0.05, 0.1 millidarcies). This table illustrates, for a given water saturation, the increased sensitivity to aqueous phase trapping that occurs as the formation permeability decreases. For example, a formation with a permeability of 0.05 millidarcies and a 50% S_{wi} , has a calculated APT_i value just below the 0.8 criteria, where significant sensitivity to aqueous phase trapping would be expected. In contrast, a lower permeability formation (0.001 md) must have a water saturation above 70% to remain above the 0.8 criteria.

Table #I-2 - Calculated Aqueous Phase Trapping Index Values [3]

Perm = 0.001 md		Perm = 0.01 md		Perm = 0.05 md		Perm = 0.1 md	
APT_i Index Value	S_{wi} Initial (fraction)	APT_i Index Value	S_{wi} Initial (fraction)	APT_i Index Value	S_{wi} Initial (fraction)	APT_i Index Value	S_{wi} Initial (fraction)
0.79	0.70	1.04	0.70	1.21	0.70	1.29	0.70
0.68	0.65	0.93	0.65	1.10	0.65	1.18	0.65
0.57	0.60	0.82	0.60	0.99	0.60	1.07	0.60
0.46	0.55	0.71	0.55	0.88	0.55	0.96	0.55
0.35	0.50	0.60	0.50	0.77	0.50	0.85	0.50
0.24	0.45	0.49	0.45	0.66	0.45	0.74	0.45
0.13	0.40	0.38	0.40	0.55	0.40	0.63	0.40
0.02	0.35	0.27	0.35	0.44	0.35	0.52	0.35
-0.09	0.30	0.16	0.30	0.33	0.30	0.41	0.30
-0.20	0.25	0.05	0.25	0.22	0.25	0.30	0.25
-0.31	0.20	-0.06	0.20	0.11	0.20	0.19	0.20
-0.42	0.15	-0.17	0.15	0.00	0.15	0.08	0.15
-0.53	0.1	-0.28	0.1	-0.11	0.1	-0.03	0.1

The water saturation values in red indicate reservoirs that will likely exhibit significant sensitivity to aqueous phase trapping.

Given that aqueous phase trapping occurs, what are the tools in BJ Service's toolbox that help us minimize aqueous phase trapping problems during completion and stimulation operations?

- Use of fluid loss control additives to minimize the amount of water lost to the formation during drilling or stimulation operations.
- Use of non-aqueous fluids (methanol-based, oil-based, or gas-based) to eliminate water injected into the formation.
- Energizing stimulation fluids with gases to "pressure charge" the near-wellbore area, enhancing formation cleanup following treatment.
- Fracturing with foamed fluids, to both reduce the amount of water in the treatment and "pressure charge" the reservoir.
- Using surfactants to lower the interfacial tension between water and gas, enhancing well cleanup.

- Adding methanol to water-based treatments to reduce water content, lower interfacial tension, and enhance the evaporation of the water-based filtrate during reservoir cleanup. Well cleanup in gas reservoirs occurs in two phases, with the first phase corresponding to the liquid production during flowback, while the second phase corresponds to the evaporation of the waterblock region with continued gas flow. Adding methanol to the completion fluid in a year-2000 laboratory study reduced the cleanup time from 40 days to 1 day.[4]

Aqueous phase trapping is a given in many reservoirs, and is particularly detrimental to cleanup in low-permeability gas reservoirs due to the high capillarity of these "tight" sandstones. In many cases, the original water saturation in these reservoirs is actually below the expected irreducible water saturation, which makes them particularly sensitive to water imbibition and hydrocarbon relative permeability reductions.

Given wireline log calculated water saturations, Table #I-2 can be used as a tool to aid in evaluating a reservoir's potential for aqueous phase trapping. This helps in the decision process as to whether specific measures (such as those described previously) should be included in the treatment design. BJ Services has multiple tools in its toolbox to address aqueous phase trapping; those tools are aimed at improving stimulation success and maximizing economic return for our clients.

[1] Erwin, C.R. Pierson, and Bennion, D.B., "Brine Imbibition Damage in the Alpine/Colville River Field, Alaska", Paper 2003-050 presented at the 54th Annual Canadian/International Petroleum Conference, Calgary Alberta, June 2003.

[2] Bennion, D.B., Thomas, F.B., Bietz, R.F., and Bennion, D.W., "Water and Hydrocarbon Phase Trapping in porous Media – Diagnosis, Prevention and Treatment", *Journal of Canadian Petroleum Technology, December 1996, page 29.*

[3] Interoffice communication with Randy LaFollette – BJ Services, Tomball

[4] Kamath, Jairam, and Laroche, Catherine, "Laboratory Based Evaluation of Gas Well Deliverability Loss Due to Waterblocking", paper SPE 63161 presented at the SPE Annual Technical Conference and Exhibition, Dallas, Texas, October 2000.

Appendix I – Core Photographs

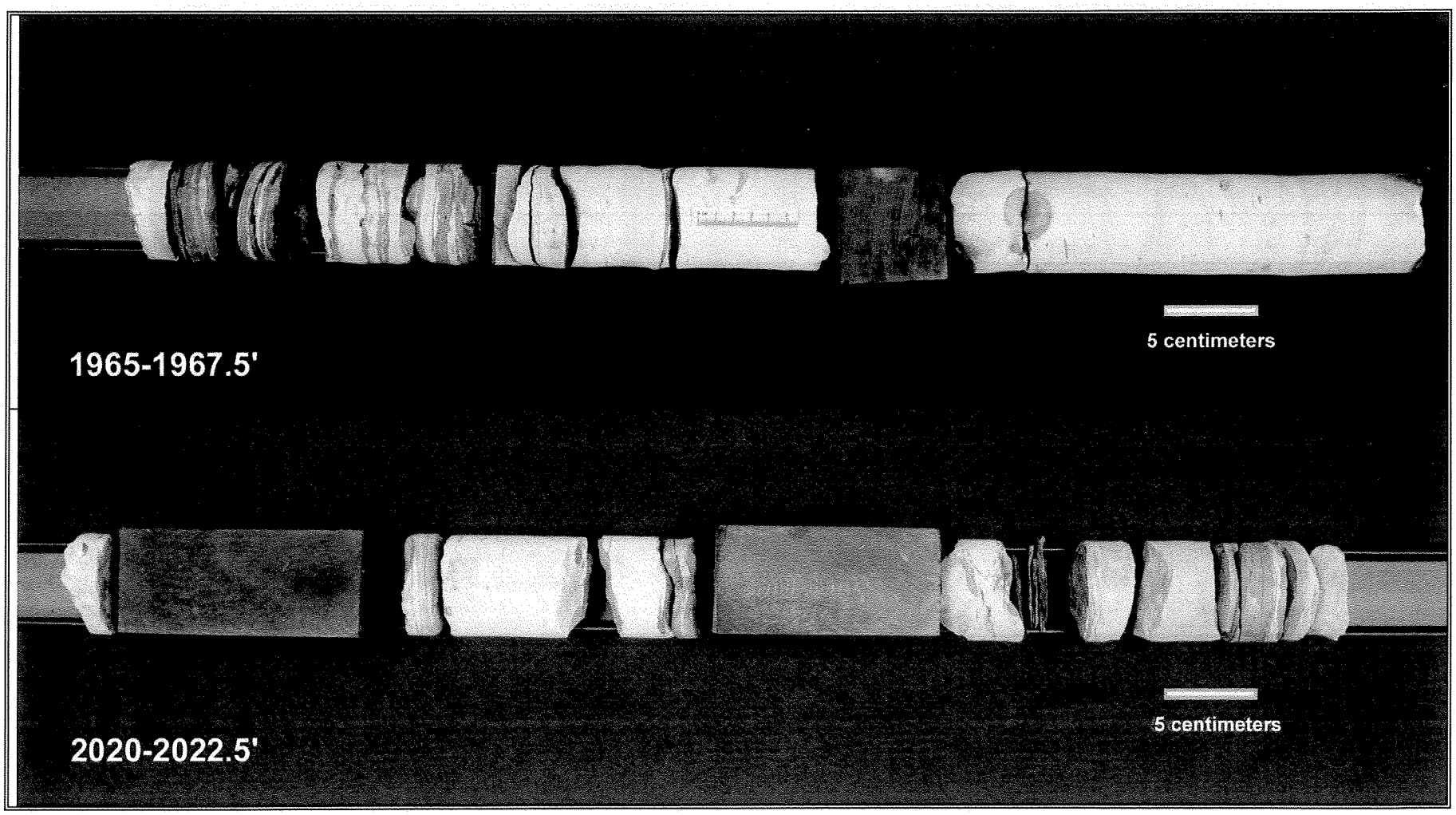

PHOTOPLATE 1 - SCANNING ELECTRON MICROSCOPE PHOTOMICROGRAPHS
Wier Formation - 1966.1

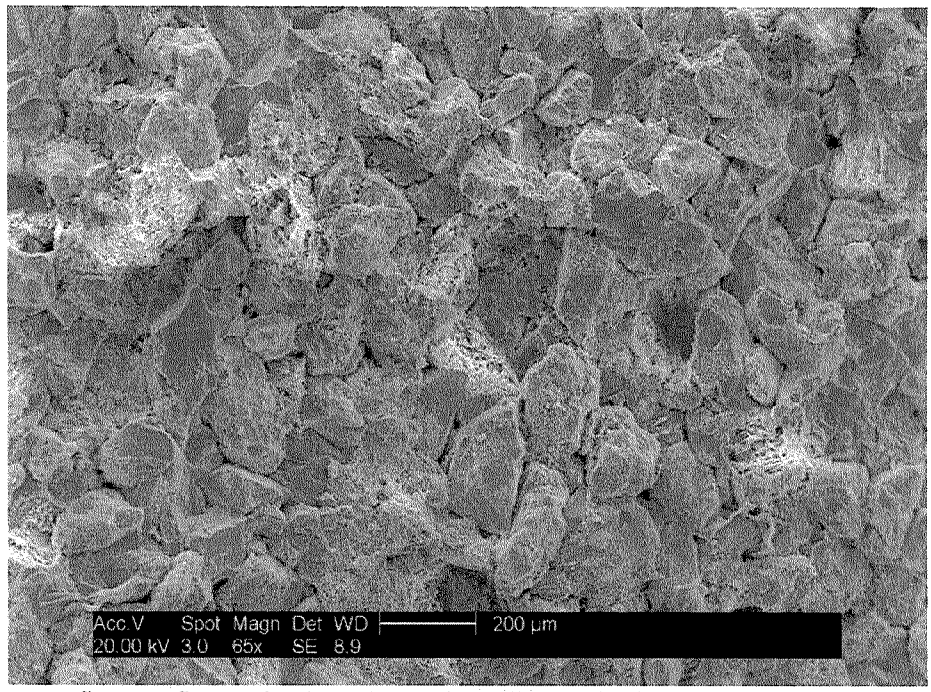

VIEW A : This very fine- to fine-grained sandstone is well sorted with intergranular porosity described as Fair. Small open intergranular pore spaces are visible throughout the sample.

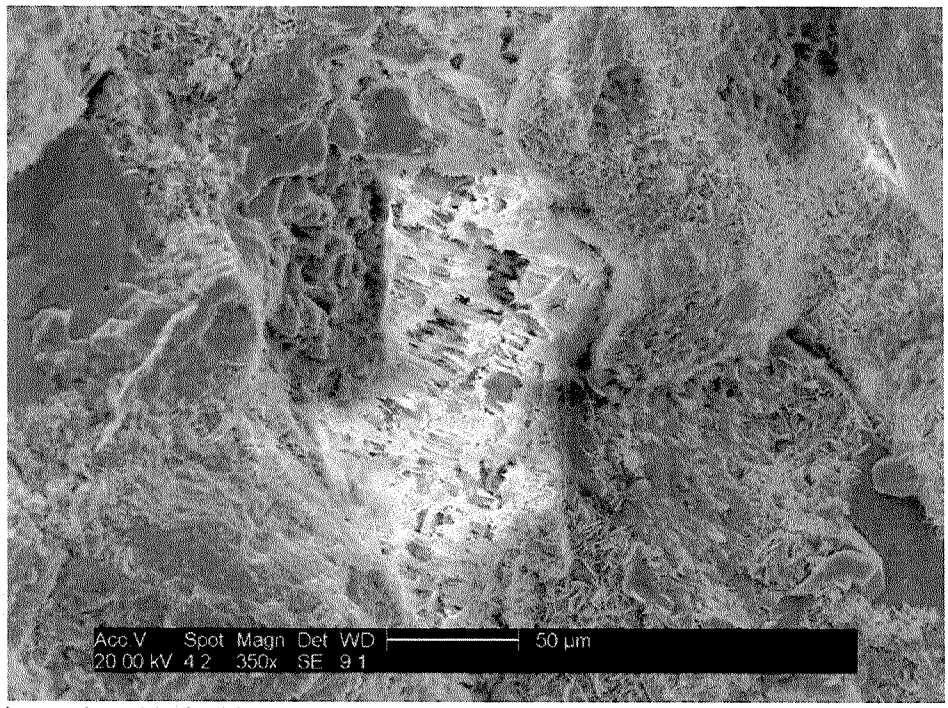

VIEW B : Grain-coating chlorite blades are the major clays, source of cementation, and contributes to total porosity through microporosity. Secondary porosity created by the partial-dissolution of the feldspar grain in the middle of the photograph effects an increased total porosity.

PHOTOPLATE 2 - SCANNING ELECTRON MICROSCOPE PHOTOMICROGRAPHS
Wier Formation - 1967.5

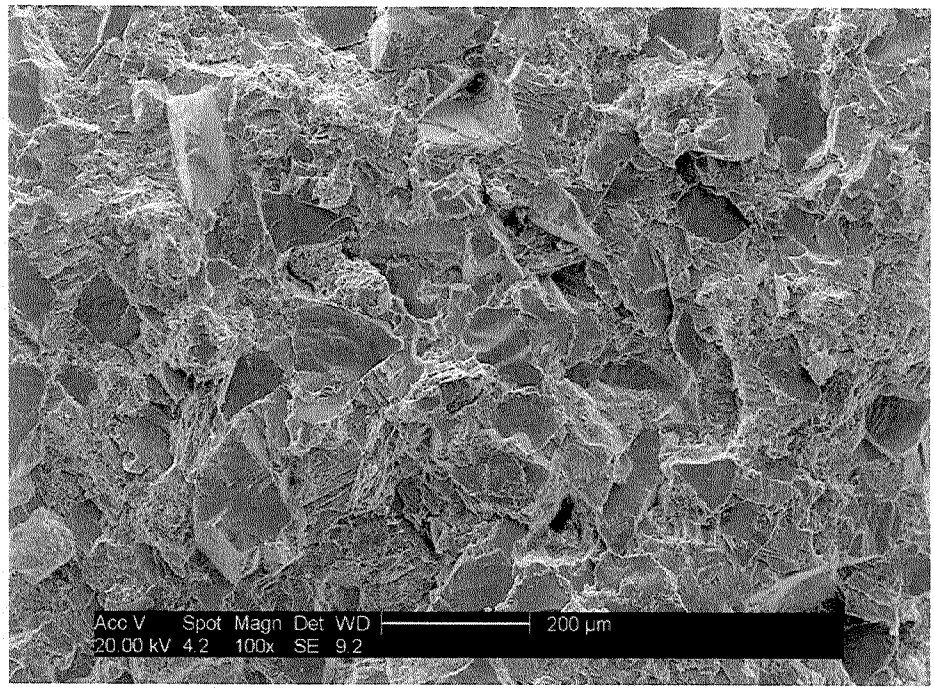

VIEW A : This calcareous, very fine- to fine-grained sandstone is interpreted to have Poor intergranular porosity. Heavy calcite cementation of framework grains leaves a very minimal amount of open pore spaces.

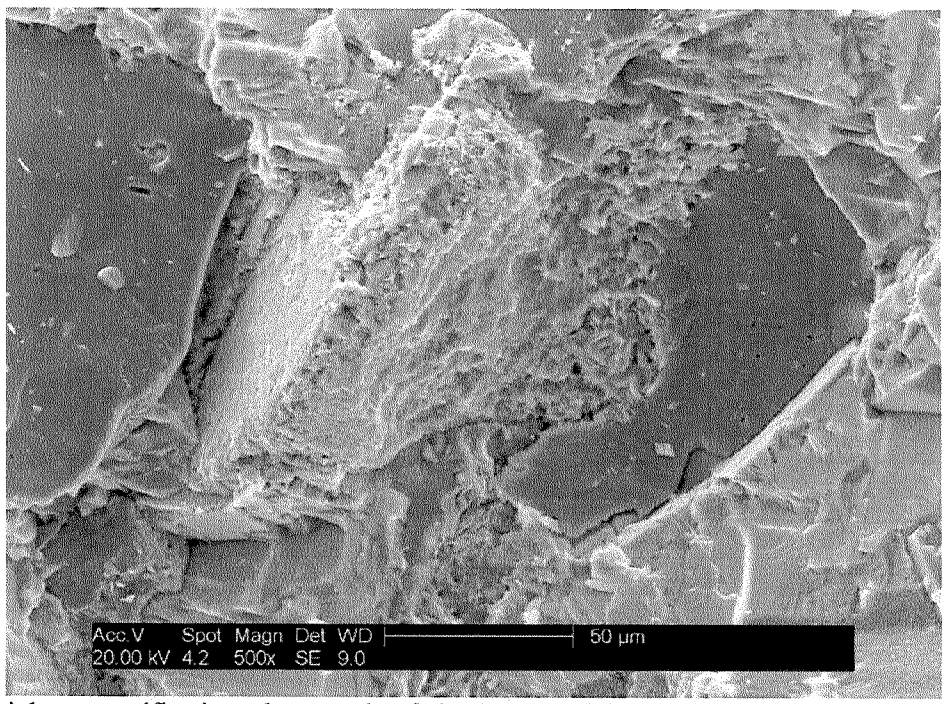

VIEW B : A higher magnification photograph of the heavy calcite cementation. XRD analysis revealed this sample to contain over 30% of carbonate cement.

PHOTOPLATE 3 - SCANNING ELECTRON MICROSCOPE PHOTOMICROGRAPHS
Wier Formation - 2021.0

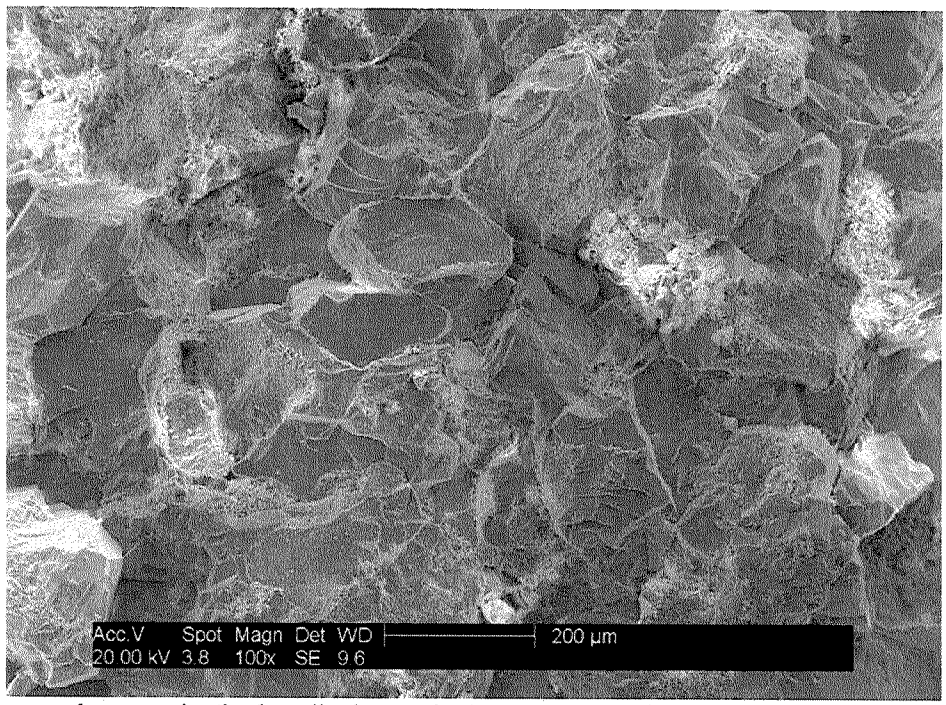

VIEW A : Intergranular porosity is described as Fair due to small open intergranular pore spaces and thin grain coatings of chlorite clay.

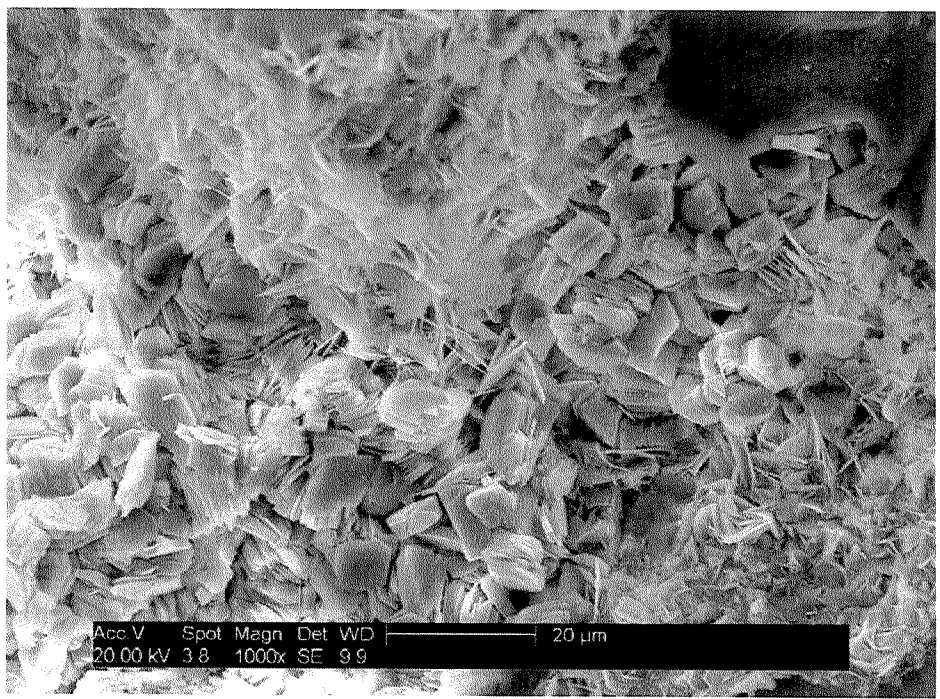

VIEW B : A high magnification photograph of a clay filled pore. At this depth, microporosity associated with pore-filling kaolinite booklets and grain-coating chlorite assume a greater proportion of total porosity.

PHOTOPLATE 4 - SCANNING ELECTRON MICROSCOPE PHOTOMICROGRAPHS

Wier Formation - 2022.0 ft.

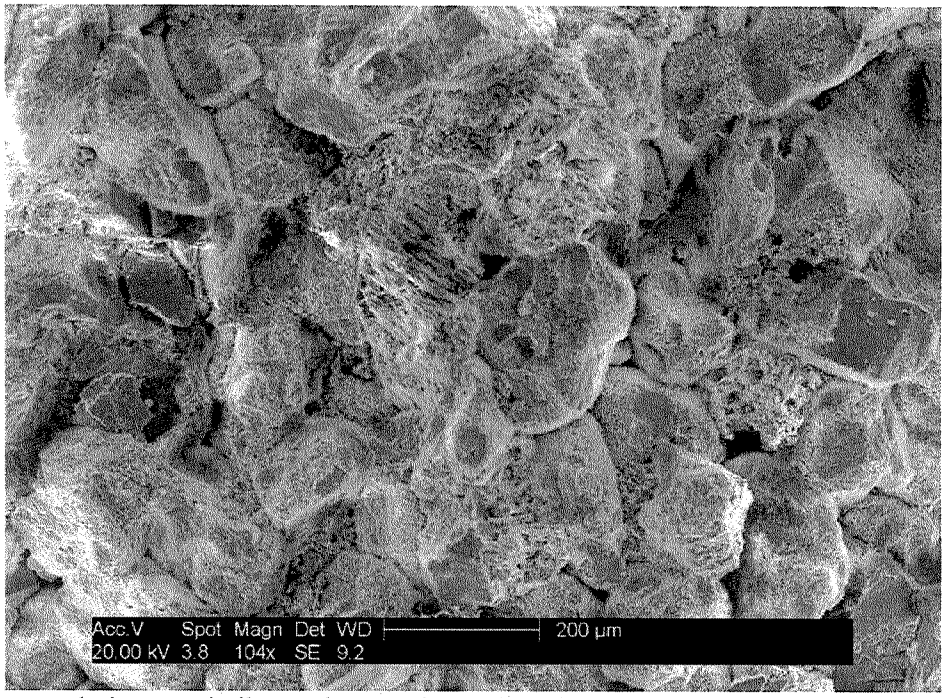

VIEW A : This sample is very similar to the sample at 2021.0'. Intergranular porosity is described as Fair with slightly more chlorite clay cementation present. The thin coating of chlorite clay can be viewed surrounding framework grains in the above photograph.

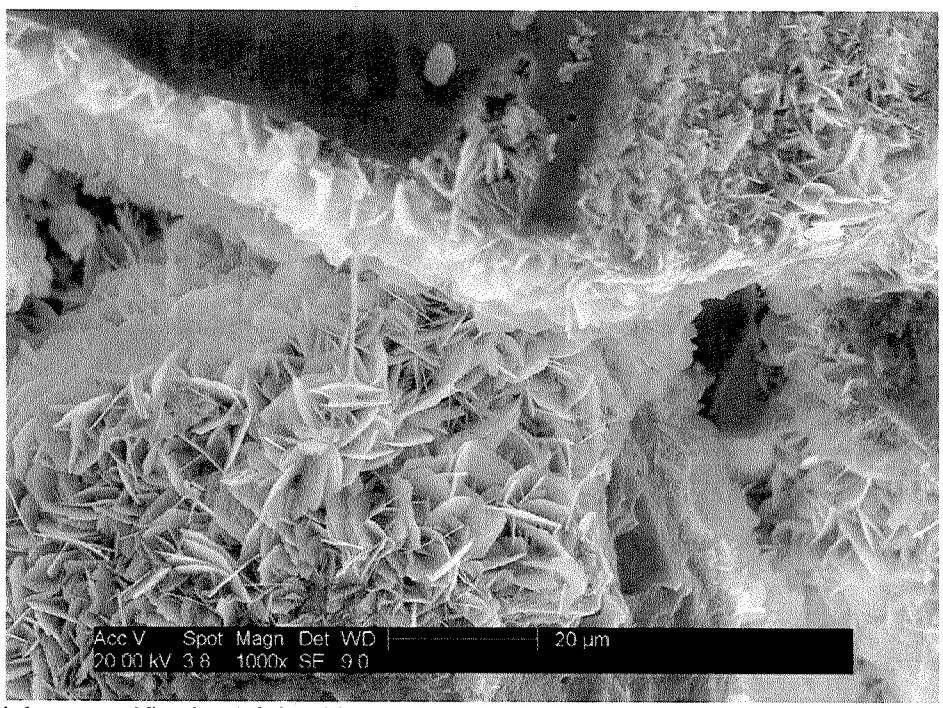

VIEW B : A higher magnification of the thin coating of chlorite clay on framework grains and the microporosity associated with the clay (between chlorite "blades").